Pygmy dipole resonance in ^{140}Ce via inelastic scattering of ^{17}O

M. Krzysiek,[1] M. Kmiecik,[1] A. Maj,[1] P. Bednarczyk,[1] A. Bracco,[2,3] F. C. L. Crespi,[2,3] E. G. Lanza,[4] E. Litvinova,[5,6] N. Paar,[7]
R. Avigo,[2,3] D. Bazzacco,[8] G. Benzoni,[2] B. Birkenbach,[9] N. Blasi,[2] S. Bottoni,[2,3] S. Brambilla,[2,3] F. Camera,[2,3] S. Ceruti,[2,3]
M. Ciemała,[1] G. de Angelis,[10] P. Désesquelles,[11] J. Eberth,[9] E. Farnea,[8] A. Gadea,[12] A. Giaz,[2] A. Görgen,[13,14] A. Gottardo,[10,15]
J. Grębosz,[1] H. Hess,[9] R. Isocarte,[8] A. Jungclaus,[16] S. Leoni,[2,3] J. Ljungvall,[11] S. Lunardi,[8,15] K. Mazurek,[1] R. Menegazzo,[8]
D. Mengoni,[17,8,15] C. Michelagnoli,[8,15] B. Milion,[2] A. I. Morales,[2,3] D. R. Napoli,[10] R. Nicolini,[2,3] L. Pellegri,[2,3] A. Pullia,[2,3]
B. Quintana,[18] F. Recchia,[8,15] P. Reiter,[9] D. Rosso,[10] M. D. Salsac,[13] B. Siebeck,[9] S. Siem,[14] P.-A. Söderström,[19,20] C. Ur,[8,10,21]
J. J. Valiente-Dobon,[10] O. Wieland,[2] and M. Ziębliński[1]

[1]*Institute of Nuclear Physics, Polish Academy of Sciences, 31-342 Kraków, Poland*
[2]*INFN Sezione di Milano, I-20133 Milano, Italy*
[3]*Dipartimento di Fisica, Università di Milano, I-20133 Milano, Italy*
[4]*INFN Sezione di Catania, I-95123 Catania, Italy*
[5]*Department of Physics, Western Michigan University, Kalamazoo, Michigan 49008-5252, USA*
[6]*National Superconducting Cyclotron Laboratory, Michigan State University, East Lansing, Michigan 48824-1321, USA*
[7]*Department of Physics, Faculty of Science, University of Zagreb, Croatia*
[8]*INFN Sezione di Padova, I-35131 Padova, Italy*
[9]*Institut für Kernphysik, Universität zu Köln, Zülpicher Str. 77, D-50937 Köln, Germany*
[10]*Laboratori Nazionali di Legnaro, INFN, I-35020 Legnaro (PD), Italy*
[11]*Centre de Spectrométrie Nucléaire et de Spectrométrie de Masse - CSNSM, CNRS/IN2P3 and Université Paris-Sud,
F-91405 Orsay Campus, France*
[12]*Instituto de Física Corpuscular, CSIC-Universidad de Valencia, E-46071 Valencia, Spain*
[13]*Institut de Recherche sur les lois Fondamentales de l'Univers - IRFU, CEA/DSM, Centre CEA de Saclay,
F-91191 Gif-sur-Yvette Cedex, France*
[14]*Department of Physics, University of Oslo, P. O. Box 1048 Blindern, N-0316 Oslo, Norway*
[15]*Dipartimento di Fisica e Astronomia dell'Università di Padova, I-35131 Padova, Italy*
[16]*Instituto de Estructura de la Materia, CSIC, Madrid, E-28006 Madrid, Spain*
[17]*Nuclear Physics Research Group, University of the West of Scotland, High Street, Paisley, PA1 2BE, Scotland, United Kingdom*
[18]*Laboratorio de Radiaciones Ionizantes, Universidad de Salamanca, E-37008 Salamanca, Spain*
[19]*Department of Physics and Astronomy, Uppsala University, SE-75120 Uppsala, Sweden*
[20]*RIKEN Nishina Center, 2-1 Hirosawa, Wako, 351-0198 Saitama, Japan*
[21]*ELI-NP, Horia Hulubei National Institute of Physics and Nuclear Engineering, Bucharest - Magurele, Romania*

The γ decay from the high-lying states of ^{140}Ce excited via inelastic scattering of ^{17}O at a bombarding energy of 340 MeV was measured using the high-resolution AGATA-demonstrator array in coincidence with scattered ions detected in two segmented ΔE-E silicon detectors. Angular distributions of scattered ions and emitted γ rays were measured, as well as their differential cross sections. The excitation of 1^- states below the neutron separation energy is similar to the one obtained in reactions with the α isoscalar probe. The comparison between the experimental differential cross sections and the corresponding predictions using the distorted-wave Born approximation allowed us to extract the isoscalar component of identified 1^- pygmy states. For this analysis the form factor obtained by folding microscopically calculated transition densities and optical potentials was used.

I. INTRODUCTION

The electric dipole ($E1$) response is one of the basic properties of atomic nuclei. Its major part is exhausted by the isovector giant dipole resonance (IVGDR) (for an overview of giant resonances see Refs. [1,2]), which is a very well-studied collective phenomenon described as an out-of-phase oscillation of protons versus neutrons, located in the energy interval well above the neutron separation energy (10–20 MeV). Below the IVGDR and around the particle separation energy, a small fraction of fragmented dipole states is also observed, exhausting a few percent of an energy-weighted sum rule (EWSR) depending on the nucleus. This additional strength is called pygmy dipole resonance (PDR).

The PDR was interpreted according to the hydrodynamical model as a collective oscillation of the neutron skin against the isospin saturated core of the nucleus [3,4]. The expected relation between pygmy states and the formation of a neutron skin has important implications in astrophysics. It is found that a correlation exists between the neutron skin thickness and the symmetry energy of the equation of state [5]. Moreover, the pygmy dipole strength plays a significant role in the prediction of radiative neutron capture rates of the r-process nucleosynthesis and thus in elemental abundance distributions [6].

The origin and properties of the pygmy dipole states are still under debate [7], given that many microscopic calculations can qualitatively reproduce the experimental data but the

dominant underlying structure of the calculated wave functions is different in various models. Additionally, the analyses of transition densities for the pygmy dipole states have shown their strong isospin mixing, being thus a common feature for these states. It is found in different microscopic models that protons and neutrons oscillate in phase at the interior of the nucleus, while at the surface only neutrons contribute. The key features of the predictions for the PDR (and of other exotic modes of excitation) are discussed in Ref. [8]. More recently, several studies concerning the description of the properties of the PDR were made and we refer to most of them in the following discussions in this paper. Experimentally, information on the strength of the PDR can be obtained in real- or virtual-photon scattering experiments. The nuclear resonance fluorescence (NRF) method has been most widely used to gain information on the $E1$ strength distribution below the neutron separation energy for a large number of nuclei, including ^{140}Ce [9]. In order to derive the details on the underlying structure of the PDR, experiments with α particles as complementary isoscalar probes were performed for several nuclei including ^{124}Sn [10] and ^{140}Ce [11]. Indeed, the comparison of the (γ,γ') and $(\alpha,\alpha'\gamma)$ reactions gave new insight into the isospin mixing of the pygmy states. While the (γ,γ') method allows us to excite the "total" strength of the PDR, the α scattering excites only the low-energy part of the pygmy states. The isoscalar character of the low-energy states [12] is inferred through their excitation with isoscalar probes. In addition, to reproduce the size of the excitation cross section one needs transition densities with behaviors typical of states corresponding to oscillations of the neutron skin. Conversely, the high-energy states are mainly of isovector nature and are associated with the tail of the GDR. These findings emphasize that the application of different probes is mandatory for a comprehensive understanding of characteristic features of the PDR. In contrast to the γ probe, using α particles or heavy ions at bombarding energies below approximately 50 MeV/u and selecting the peripheral scattering, one is more sensitive to the target nucleus surface. The calculations [13] performed for the systems $\alpha + ^{90}$Zr, ^{208}Pb, and ^{17}O + ^{90}Zr, ^{208}Pb have shown a much higher nuclear contribution to the excitation of isoscalar GDR as compared with Coulomb interaction. Furthermore, it was demonstrated that the excitation using ^{17}O at 20 MeV/u is dominated by nuclear interaction. This allowed us to conclude that the ^{17}O at 20 MeV/u can be considered as an effective isoscalar probe. Therefore, the choice of this projectile ensures sensitivity to the isoscalar part of the pygmy states. Furthermore, due to the low neutron binding energy in ^{17}O (4.1 MeV), the detection of the projectile allows clean measurements of the γ radiation from the target nucleus, especially in the PDR energy region ($E_x > 4$ MeV). For this reason, it is more preferable to use ^{17}O than the more abundant isotope ^{16}O (purer as an isoscalar probe) [13]. Recent experiments performed on the ^{208}Pb [14], ^{124}Sn [15], ^{140}Ce [16], and ^{90}Zr [17] nuclei have shown that the $(^{17}$O$,^{17}$O$'\gamma)$ reaction at $\approx$20 MeV/u is a good tool for investigating the isospin properties of the pygmy dipole states. A recent overview is in Ref. [13].

This paper reports on the study of pygmy states in ^{140}Ce using the $(^{17}$O$,^{17}$O$'\gamma)$ reaction. The general aim is

to investigate the structure of the pygmy states, in particular their isospin mixing by comparison with previous data from (γ,γ') and $(\alpha,\alpha'\gamma)$ experiments. The more specific goal is to compare the experimental data with calculations based on the distorted-wave Born approximation (DWBA) and using a form factor obtained by double folding a nucleon-nucleon potential with microscopically calculated transition densities [18,19]. This allows us to extract a fraction of the isoscalar energy-weighted sum rule (ISEWSR) exhausted by pygmy states for the ^{140}Ce nucleus.

II. EXPERIMENT

The ^{17}O beam at an energy of 20 MeV/u was delivered by the PIAVE-ALPI accelerator system of the Legnaro National Laboratories. The ^{140}Ce target used had a thickness of 2.5 mg/cm^2. The ^{17}O ions were chosen to avoid the background from γ rays due to projectile excitation. The scattered ^{17}O nuclei were detected by two ΔE-E silicon telescopes of the TRACE array [20], mounted inside a scattering chamber at an angle of $9°$ with respect to the beam axis on the left and right sides. The telescopes consisted of two segmented Si-pad detectors, each made of 60 pixels (with a pixel size of 4×4 mm^2). The resulting solid angle for the Si telescope was 100 msr. The excitation of the target nucleus was followed by emission of γ rays measured by five triple clusters of high-purity germanium (HPGe) detectors of the AGATA-Demonstrator array [21–23]. For the events from the AGATA-Demonstrator it was necessary to use advanced algorithms in order to fully profit from a good position resolution of the segmented Ge detectors. At first, the pulse shape analysis (PSA) [23] allowed us to identify points of interaction of a γ ray scattering in the Ge crystals. Second, the reconstruction of the path of the γ rays inside the detector was performed with the Mars Gamma Tracking (MGT) algorithm [24]. Such an approach resulted in reconstruction of the γ-ray emission angle from the target nucleus with the remarkable precision of $1°$. It was therefore possible to perform very accurate Doppler correction which was crucial for the analysis of high-energy lines in γ-ray spectra. Some advantages of the good angular resolution of AGATA are underlined in this paper, in connection with the discussion on the data for the angular distributions of emitted γ rays and for the differential cross sections.

III. RESULTS

The first part of the data analysis was aimed at identifying the ^{17}O scattering channel using the silicon detector responses. This was done by plotting for each pixel of the Si detectors a two-dimensional histogram of the energy deposited in the first layer of the Si detectors (ΔE) versus the total kinetic energy (E_{TKE}) deposited in both layers. Such a matrix for one pad of Si detectors is shown in Fig. 1(a). One can observe a clear separation between different isotopes.

Because the velocity of the target nucleus was at the level of 0.5% of the speed of light, the Doppler shift was not negligible, and the correction for the energy of the γ rays emitted from ^{140}Ce was performed event by event. The angle for the velocity vector of the target nucleus was deduced from the reaction
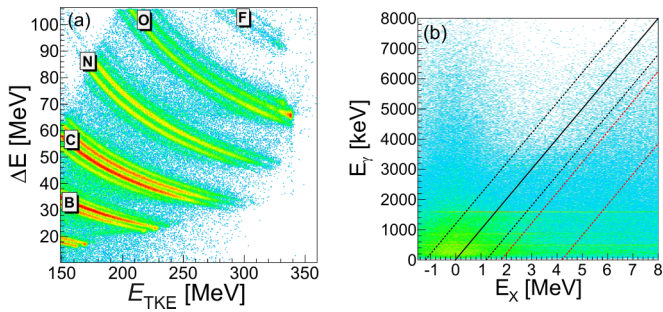
FIG. 1. Two-dimensional histograms of (a) the energy deposited in the first layer of Si detector (ΔE) versus the total kinetic energy deposited in both layers (E_{TKE}) and (b) the excitation energy (E_x) versus energy of the γ rays measured with the AGATA (E_γ). The diagonal gates (width of 2.4 MeV) corresponding to the decays to ground state ($E_\gamma = E_x$) and higher-lying states ($E_\gamma = E_x + 3$ MeV) are indicated.
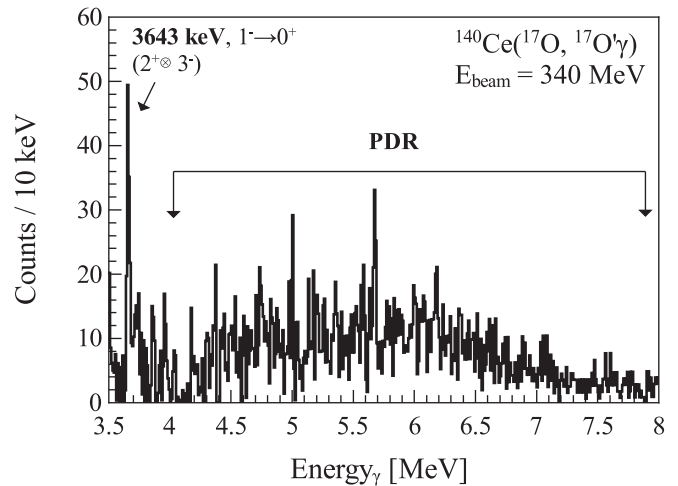

FIG. 2. γ-ray energy spectrum in the PDR region measured with the AGATA demonstrator array in coincidence with the ^{17}O inelastic scattering and with a selection of γ rays deexciting to the ground state.

kinematics knowing the position of the ^{17}O ion detected in the Si detectors.

The pygmy dipole resonance is expected to be composed of a number of discrete 1^- states decaying predominantly to the ground state. In order to select only such states, the γ-ray energy must be equal to the excitation energy. This requirement can be fulfilled by constructing the coincidence matrix between the energy of the emitted γ rays versus the excitation energy. In this case, a two-dimensional histogram of the γ-ray energy measured in AGATA and the total kinetic energy deposited in the silicon detectors was constructed [see Fig. 1(b)] and then a diagonal gate ($E_\gamma = E_x$) with a width of ± 1.2 MeV was applied. The limited energy resolution of the Si detectors implied the possible presence of unwanted events in the selected region of interest, namely, that corresponding to ground-state decays (central diagonal gate). Indeed an almost exponential "background" seems to be present in the spectrum corresponding to the central diagonal cut, which could be due to decays to high-lying states. Therefore a spectrum associated with a second diagonal cut in a region at a higher excitation energy was constructed and considered as a "background" to be subtracted. Such a "background spectrum" has an exponential shape and it dies out in the region of the pygmy states. The spectrum shown in Fig. 2 was obtained with such a background subtraction procedure. One notes the presence of a number of discrete states that were identified before using (γ, γ') and ($\alpha, \alpha' \gamma$) reactions. For the first state at 3643 keV, evidence was found that it has a two-phonon ($2^+ \otimes 3^-$) character [25], and this is further discussed in Ref. [26]. In the following, one sees that also the excitation cross section of this state is different from the PDR states. The peak at around 5 MeV is likely to be a transition from either a 2^+ state or a 3^- state at 4979 keV, which was observed in the ^{142}Ce(p, t) experiment [27]. This is consistent with the findings from NRF experiments, in which there were no 1^- peaks identified at this energy. In our experiment, due to very limited statistics, it is not possible to perform the angular distributions analysis for this single peak.

Exploiting the position sensitivity of the AGATA and Si detectors it was possible to reconstruct the γ-ray emission

angles from the recoiling ^{140}Ce nucleus and thus to extract the angular distributions of the emitted γ rays. The results for the dipole ($E1$, 868 keV: $3^- \rightarrow 2^+$) and quadrupole ($E2$, 1596 keV: $2^+ \rightarrow 0^+$) γ transitions are presented in Fig. 3. The result shows the high sensitivity of our data set to transition multipolarities. The expected trends for the $E1$ and $E2$ transitions were calculated using the equations given in Ref. [28]. It should be noted that the data points at angles larger than $90°$ are rather scattered and that the low statistics of these points does not fully explain this behavior. Indeed, one cannot exclude other effects such as some more complicated reaction mechanisms showing up at these large angles or some extra inefficiencies of the Si pads at these angles not entirely accounted for in the computed error bars. Therefore the angular distribution data between $90°$ and $180°$ were disregarded in the following analyses. After choosing the angular intervals corresponding to the dipole ($65°$-$115°$) and quadrupole ($15°$-$65°$) transitions, it was possible to obtain the γ spectra according to their multipolarity. The bottom panel of Fig. 3 shows the ratio of counts for the $E1$ and $E2$ transitions for two transitions at 868 and 1596 keV as well as in the pygmy energy region from 4 to 8 MeV with 1-MeV intervals. The data in the pygmy region are found to have a dominant dipole character.

One aim of this study is to measure the cross section for the excitation of the PDR states using the ^{17}O probe and to compare it with the previous results from (γ, γ') [9] and ($\alpha, \alpha' \gamma$) [11] experiments. Due to very low statistics in the pygmy energy region, the analysis for the individual peaks is very difficult. In most cases, the identification of the position of the peaks is only possible by comparison with the results from previous (γ, γ') and ($\alpha, \alpha' \gamma$) experiments. No additional background estimation was done after the procedure of background subtraction described before. Figure 4(a) shows the differential cross section corresponding to the scattering angle of $12.5°$ (in c.m. frame of reference) from the present work. Figure 4(b) shows the single cross sections (after
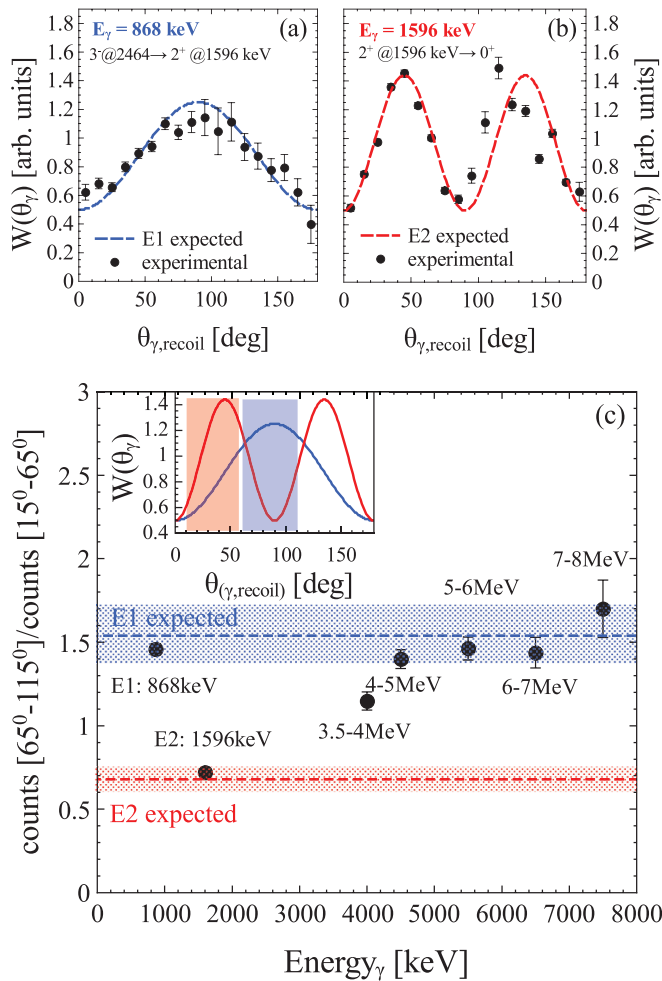
FIG. 3. Angular distributions of γ rays emitted by the ^{140}Ce nucleus. (a) Dipole ($E1$) γ transition at 868 keV ($3^- \rightarrow 2^+$) together with the expected trend (blue line). (b) Quadrupole ($E2$) γ transition at 1596 keV ($2^+ \rightarrow 0^+$) and the corresponding expected trend (red line). (c) Ratio between the number of counts in the 65°-115° angular range (blue region in the inset) and the 15°-65° angular range (red region in the inset) for different transitions. The blue and red bands show the range of values expected for pure $E1$ and $E2$ transitions, respectively.

FIG. 4. Experimental cross sections of 1^- states in ^{140}Ce excited via inelastic scattering of ^{17}O (a) compared to the cross sections measured in $(\alpha,\alpha'\gamma)$ [11] (b) and the values of $B(E1)$ obtained in a NRF experiment [9] (c).

integration of the double-differential cross section over the α-γ angular correlation) obtained in the $(\alpha,\alpha'\gamma)$ experiment of Ref. [11]. Figure 4(c) gives the $B(E1)$ values obtained in the NRF experiment of Ref. [9]. Due to limited statistics, it was not possible to distinguish between the two transitions at 5157 and 5190 keV, and the two transitions at 5548 and 5574 keV. In these cases, the two peaks were treated as one and the measured cross section reflects the sum of the pair. Similar to what was observed in the $(\alpha,\alpha'\gamma)$ experiment, it was not possible to identify discrete peaks for excitation energies higher than 6.2 MeV, supporting the conclusion that isoscalar probes excite only the low-energy part of the pygmy states.

To describe the pygmy dipole excitation cross section, a DWBA analysis was performed for the present data using the FRESCO code [29]. The approach requires the optical potential to describe the incoming and outgoing waves and a form factor
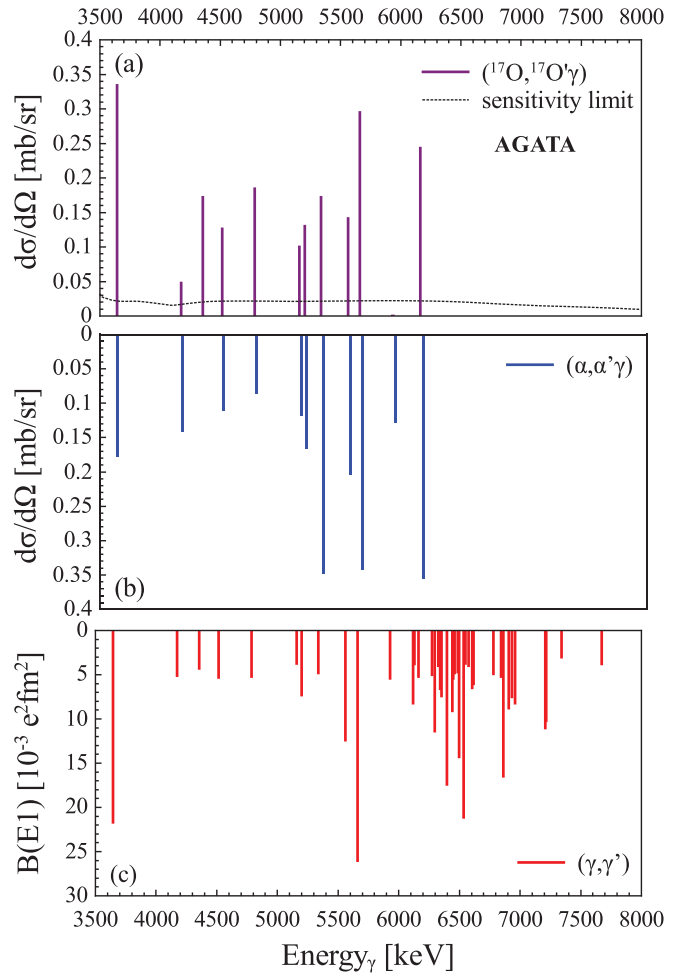
containing information on the nuclear structure characterizing the reaction [30,31]. For the elastic calculations, the code uses the two-body wave function and the optical potential, which describes the nuclear interaction between the projectile and target nuclei. In this way, the effective interaction is a sum of the Coulomb and nuclear optical potentials. For the calculations of the elastic scattering cross sections, the optical potential was assumed to be of Woods-Saxon type. The cross sections for excitations of collective states were calculated using the deformed optical potential model, which includes the Coulomb and nuclear potentials for the angular momentum transfer L. To calculate the inelastic excitations, the code refers to the collective model for the nuclear part of the effective interaction. A deformation is associated with the excited levels though a quantity denoted as the reduced deformation length, which is calculated starting from the reduced transition probability, $B(EL)\uparrow$ [29]. In Fig. 5(a) the data for elastic scattering divided by the Rutherford cross section are shown. The experimental data are normalized to the DWBA calculations in order to take into account the beam current and target thickness. This normalization
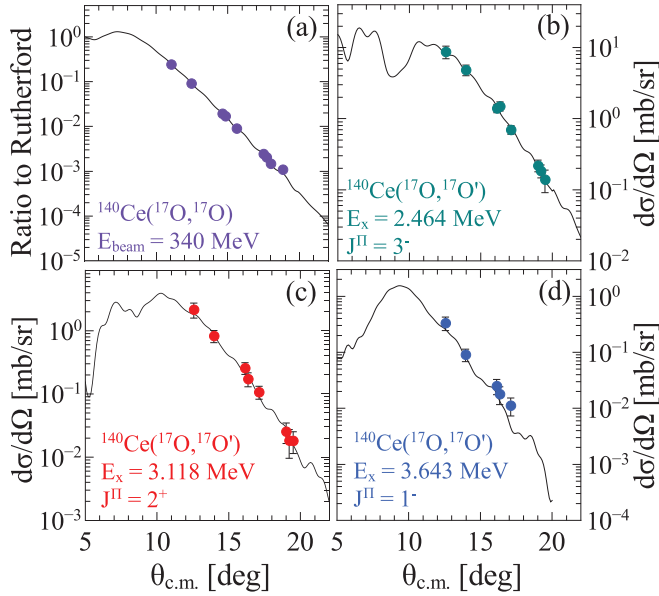
FIG. 5. Cross-section measurements (filled circles) and DWBA predictions (solid curves) for the ^{140}Ce(^{17}O, ^{17}O)^{140}Ce and ^{140}Ce(^{17}O, ^{17}O′)^{140}Ce at $E_{\text{beam}} = 340$ MeV in the center-of-mass frame. (a) Elastic-scattering cross section divided by the Rutherford cross section. Other panels show cross sections for the excited states at 2.464 MeV (3^- state), 3.118 MeV (2^+ state), and 3.643 MeV (1^- state). The error bars represent the statistical error.

was used for the further analysis of inelastic excitations. The following optical model parameters of the Woods-Saxon potentials that best fitted the elastic scattering data were employed: for the depth of the real and imaginary potentials, we used $V = 48.1$ MeV and $W = 34.1$ MeV, and for the radii and the diffusenesses of the real and imaginary parts we used $r_v = r_w = 1.15$ fm and $a_v = a_w = 0.69$ fm, respectively. The Coulomb radius parameter was $r_c = 1.2$ fm. The same optical model parameters from the elastic scattering were then used to calculate the excited-state differential cross sections. The predictions for the 2^+ states at 1.596 and 3.118 MeV and the 3^- state at 2.464 MeV (see Fig. 5) were calculated using the known $B(E2)\uparrow$ and $B(E3)\uparrow$ values [32] and, moreover, pure isoscalar excitation was assumed, implying that the ratio of the neutron matrix element M_n and the proton matrix element M_p is given by $M_n/M_p = N/Z$. For the 3^- state the yield was the sum of the ground-state decay plus the branching to the 2^+ state. The data are reproduced very well and this supports the fact that these states have a collective nature. In particular also the state of the $2^+ \otimes 3^-$ character at 3643 keV is rather well reproduced with this approach [see Fig. 5(d)].

The first step analysis of 1^- states was also made using this approach. The corresponding calculations are shown in Fig. 6 with the long-dashed and short-dashed lines. The data shown in Fig. 6 correspond to the cross section of one state at 5.660 MeV [Fig. 6(b)] and to the sum of the cross sections for all the states in the regions: 4–6.2 MeV [Fig. 6(c)] and 6.2–7.8 MeV [Fig. 6(d)] representing the low- and high-energy parts of the PDR states, respectively. The cross sections for the
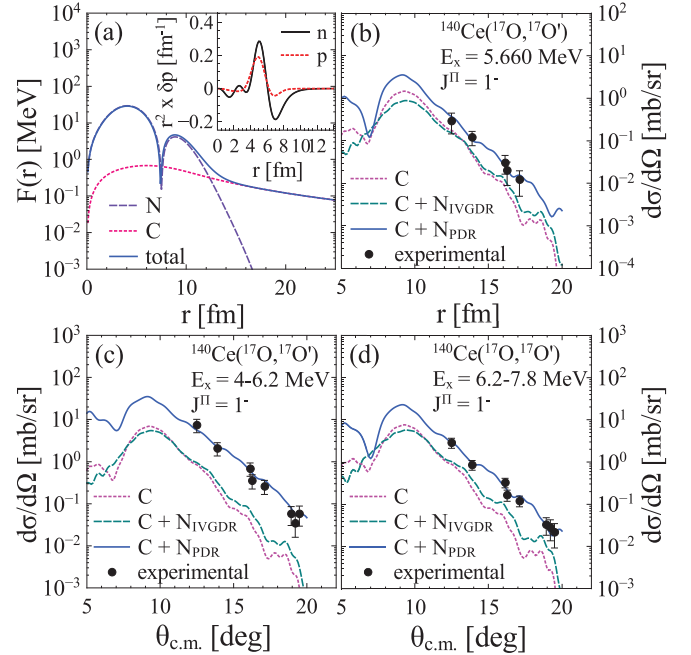

FIG. 6. Experimental cross sections for the PDR γ transition at (b) 5660 keV, and the integrated regions (c) below and (d) above 6.2 MeV of ^{140}Ce measured in the (^{17}O, ^{17}O′γ) experiment. The dotted purple line represents the Coulomb cross section calculated with the DWBA while the dashed green line is the total cross section using the standard collective form factor. The solid blue line represents the total cross section using the microscopic nuclear form factors of (a).

excitation of discrete states and levels, which correspond to the integrated regions, were obtained from our measurement and compared with the DWBA results. For the calculations, values of 0.061 and 0.121 W.u. for the sum of $B(E1)\uparrow$ strength in the low- and high-energy regions, respectively, were used as known from the NRF experiment of Ref. [9]. The standard collective form factor of IVGDR type [29] was used in order to account for the nuclear part of the interaction. It is clearly seen that such DWBA calculations account only for a small fraction of measured cross sections (12% and 42% for the low- and high-energy regions, respectively), which may suggest that the main contribution comes from the nuclear part and that a proper form factor is needed. This is also an indication for a predominantly isoscalar character of the PDR states, especially in the low-energy region. To check this assumption, we performed DWBA calculations using a microscopically calculated form factor based on transition densities for the pygmy states [see Fig. 6(a)]. The proton and neutron transition densities, obtained using the fully consistent relativistic quasiparticle random phase approximation (RQRPA) model [12] for a state at 8.39 MeV are shown in the Fig. 6(a) inset. It shows typical features of the PDR states: neutron and proton transition densities are in phase in the interior and there is a strong surface contribution due only to neutrons.

The form factor obtained with the double folding method using the M3Y nucleon-nucleon interaction [18,19] is also

TABLE I. Isoscalar energy-weighted sum rule (ISEWSR) and PDR strength (S_{IS}) determined from the present measurement.

| Energy (keV)	ISEWSR (%)	S_{IS} ($10^2 e^2$ fm^6)
4147	0.014(19)	0.83(1.12)
4355	0.039(32)	2.21(1.81)
4514	0.029(22)	1.58(1.20)
4787	0.050(40)	2.57(2.06)
5157	0.030(34)	1.43(1.63)
5190 & 5211	0.033(28)	1.56(1.33)
5337	0.053(42)	2.45(1.94)
5548 & 5574	0.038(36)	1.68(1.60)
5660	0.075(44)	3.27(1.92)
5929	Not observed	
6160	0.076(68)	3.04(2.72)

FIG. 7. Isoscalar strength distribution obtained for the PDR energy region, integrated in bins of 200 keV. The green lines correspond to the known discrete γ transitions. The pink bars give the total strength (including the unresolved part) corresponding to the total counts in each energy bin.

shown in Fig. 6(a). The microscopic nuclear form factor was then used in the DWBA analysis. For each studied PDR excitation with a given energy, the form factor was scaled for the different ISEWSR value that is exhausted by the transition. The known theoretical value from RQRPA calculations that was used as a reference was 4.14% for the PDR state at 8.39 MeV [12]. The whole energy region was then divided into bins of 200 keV, and for each bin, the ISEWSR was estimated using the procedure described above. Our results are 1.42(22)% and 0.61(14)% for the low- and high-energy regions, respectively, with a total 2.03(26)% including the unresolved strength. Then, the ISEWSR was also estimated with the same procedure for each identified PDR state and the results are shown in Table I. The summed strength in the discrete peaks was 0.44(12)%.

Finally, we deduced the isoscalar strength (S_{IS}) in units of e^2 fm^6/MeV with the same fitting procedure as for ISEWSR and knowing the theoretical value of 1.2×10^4 e^2 fm^6 for the state at 8.39 MeV. The results for each identified pygmy dipole state are given in Table I. The summed strength in all discrete peaks was therefore equal to $0.20(6) \times 10^4$ e^2 fm^6. The same procedure was applied to the total strength (including the unresolved region) giving the values of $0.66(10) \times 10^4$ and $0.22(5) \times 10^4$ e^2 fm^6 for the low- and the high-lying regions, respectively. The total strength was found to be equal to $0.88(11) \times 10^4$ e^2 fm^6. Figure 7 shows the total strength values (in 200-keV intervals) together with the discrete peaks indicated with the narrow bars.

It is interesting to compare the values of the ISEWSR for the ^{140}Ce nucleus with those deduced for the ^{124}Sn nucleus. The two experiments used the same experimental setup. The measured ISEWSR in the pygmy region for the ^{124}Sn case in the discrete peaks (low-energy region) was 2.2($\pm$0.3)% and for the whole energy region (including the unresolved region), 7.8($\pm$0.7)% [15]. The ratio of the ISEWSR for ^{124}Sn and ^{140}Ce is therefore 2.2%/0.44% = 5 for the discrete peaks. As one can observe in the ($\alpha,\alpha'\gamma$) experiments, the ratio of the cross sections for the excitation of the PDR in ^{124}Sn [10] and ^{140}Ce [11] was 10.77 (mb/sr)/2.19 (mb/sr) = 4.92 which agrees very well with our findings. This consistency between the results obtained using our (^{17}O,^{17}O'γ) method
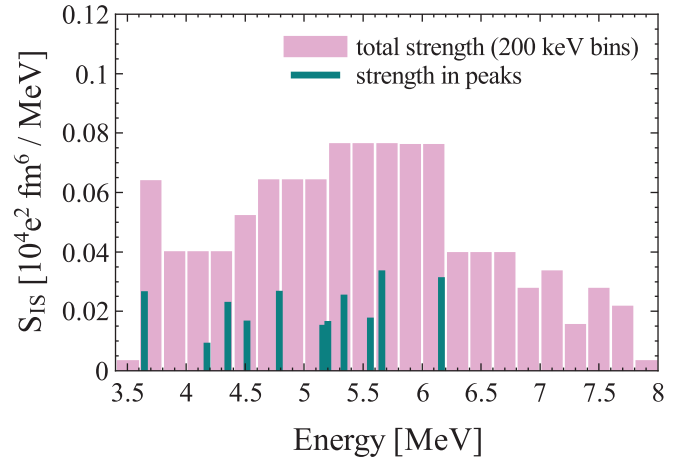
for different nuclei allows us to conclude that this probe at 20 MeV/u is a useful tool for extracting the isoscalar component of the excitation [13]. Concerning the predictions of the isoscalar strength it is important to note that transition densities for the PDR states in ^{124}Sn were obtained with a relativistic quasiparticle time blocking approximation (RQTBA) microscopic model [33].

Our experimental values as well as the ones predicted by RQRPA and RQTBA models are shown in Table II. In the case of the RQRPA calculations, all the strength is accumulated in one peak at the energy of 8.39 MeV, while in RQTBA it is fragmented into a few peaks up to 8.8 MeV.

One can notice that the measured ISEWSR for the total PDR strength, which can be considered as an upper limit of our experiment, is below the predictions of the two models, but close to the RQTBA. It should be noted that all the calculations predict the pygmy dipole states at higher energies as compared to the experimental observations. In the case of RQRPA, the difference is around 3 MeV, and all the strength is accumulated in one peak so that the fragmentation of the PDR is not reproduced [12]. It has been found that the pygmy mode, arising in the RQRPA as a single state with isoscalar character, is strongly fragmented over many states in a broad energy region due to the coupling to phonons. As a result, some fraction of the strength is located well below the original position of

TABLE II. Values of the isoscalar energy weighted sum rule (ISEWSR) and its strength (S_{IS}) obtained in this experiment compared to corresponding calculations using RQRPA [12] and RQTBA models.

Method		ISEWSR (%)	S_{IS} (10^4 e^2 fm^6)
(^{17}O,^{17}O'γ)	In peaks	0.44(12)	0.20(6)
	Total	2.03(26)	0.88(11)
RQRPA (DD-ME2)		4.14	1.2
RQTBA (NL3)		2.5	1.16

the RQRPA pygmy mode. In case of ^{140}Ce it is difficult to reproduce the fragmentation of the pygmy dipole states as the relativistic RQRPA calculations largely overestimate the energy of the lowest 2^+ phonon. The RQTBA model, which additionally takes into account the coupling to the low-energy surface phonons, is able to reproduce the fragmentation to some extent, but also overestimates the PDR energy by about 2 MeV. It was discussed, e.g., for the ^{116}Sn case [34] that for the lowest RQTBA states the transition densities look similar to the RQRPA ones, but because of the fragmentation, the amplitude of the density oscillations is about a factor of 3 smaller. However, since there are more states, in total they can effectively give a similar contribution to the cross section. Therefore, it is reasonable enough to use RQRPA transition densities as we did in our form factor calculations.

IV. SUMMARY

This paper has presented the results of a study on the isospin character of the dipole states below the particle threshold in the ^{140}Ce nucleus using inelastic scattering of ^{17}O at 20 MeV/u. The obtained differential cross sections for the excitation of pygmy dipole states are found to be in a good agreement with the ones previously measured using the $(\alpha, \alpha' \gamma)$ reaction, which confirms the selectivity in excitation of such states as compared with (γ, γ'). A DWBA analysis for the pygmy dipole states using microscopically calculated form factors based on the transition densities obtained with RQRPA allowed us to extract the fraction of the isoscalar energy weighted sum rule and its strength. The results for ^{140}Ce were compared to the ones obtained for ^{124}Sn with the same $(^{17}$O, ^{17}O$' \gamma)$ reaction

and also with the $(\alpha, \alpha' \gamma)$ reaction. High consistency of the results is observed, which allows us to conclude that inelastic scattering of ^{17}O at 20 MeV/u is a very good tool for studying the isospin character of the pygmy dipole resonance. The overestimation of our experimental ISEWSR as compared with the RQRPA predictions might be caused by the fact that RQRPA calculations do not take into account the effects of coupling to low-energy surface phonons. However, the ISEWSR value predicted by the RQTBA approach for the PDR is 2.5%, which is consistent with the 2.03% value measured as an upper limit in our experiment.

[1] P. F. Bortignon, A. Bracco, R. A. Broglia, *Giant Resonances: Nuclear Structure at Finite Temperature* (Harwood Academic, Amsterdam, 1998).

[2] M. N. Harakeh and A. van der Woude, *Giant Resonances: Fundamental High-Frequency Modes of Nuclear Excitation* (Oxford University, Oxford, 2001).

[3] R. Mohan, M. Danos, and L. C. Biedenharn, Phys. Rev. C **3**, 1740 (1971).

[4] Y. Suzuki, K. Ikeda, and H. Sato, Prog. Theor. Phys. **83**, 180 (1990).

[5] B. A. Brown, Phys. Rev. Lett. **85**, 5296 (2000).

[6] S. Goriely, Phys. Lett. B **436**, 10 (1998).

[7] D. Savran, T. Aumann, and A. Zilges, Prog. Part. Nucl. Phys. **70**, 210 (2013).

[8] N. Paar, D. Vretenar, E. Khan, and G. Colò, Rep. Prog. Phys. **70**, 691 (2007).

[9] S. Volz, N. Tsoneva, M. Babilon, M. Elvers, J. Hasper, R.-D. Herzberg, H. Lenske, K. Lindenberg, D. Savran, and A. Zilges, Nucl. Phys. A **779**, 1 (2006).

[10] J. Endres, D. Savran, P. A. Butler, M. N. Harakeh, S. Harissopulos, R. D. Herzberg, R. Krucken, A. Lagoyannis, E. Litvinova, N. Pietralla, V. Y. Ponomarev, L. Popescu, P. Ring, M. Scheck, F. Schluter, K. Sonnabend, V. I. Stoica, H. J. Wortche, and A. Zilges, Phys. Rev. C **85**, 064331 (2012).

[11] J. Endres, D. Savran, A. M. van den Berg, P. Dendooven, M. Fritzsche, M. N. Harakeh, J. Hasper, H. J. Wörtche, and A. Zilges, Phys. Rev. C **80**, 034302 (2009).

[12] N. Paar, Y. F. Niu, D. Vretenar, and J. Meng, Phys. Rev. Lett. **103**, 032502 (2009).

[13] A. Bracco, F. C. L. Crespi, and E. G. Lanza, Eur. Phys. J. A **51**, 99 (2015).

[14] F. C. L. Crespi *et al.*, Phys. Rev. Lett. **113**, 012501 (2014).

[15] L. Pellegri *et al.*, Phys. Lett. B **738**, 519 (2014).

[16] M. Krzysiek *et al.*, Phys. Scr. **89**, 054016 (2014).

[17] F. C. L. Crespi *et al.*, Phys. Rev. C **91**, 024323 (2015).

[18] E. G. Lanza, A. Vitturi, M. V. Andrés, F. Catara, and D. Gambacurta, Phys. Rev. C **84**, 064602 (2011).

[19] E. G. Lanza, A. Vitturi, and M. V. Andrés, Phys. Rev. C **91**, 054607 (2015).

[20] D. Mengoni *et al.*, Nucl. Instrum. Methods A **764**, 241 (2014).

[21] S. Akkoyun *et al.*, Nucl. Instrum. Methods A **668**, 26 (2012).

[22] A. Gadea *et al.*, Nucl. Instrum. Methods A **654**, 88 (2011).

[23] F. C. L. Crespi, *et al.*, Nucl. Instrum. Methods Phys. Res., Sect. A **705**, 47 (2013).

[24] D. Bazzacco, "mgt" (Mars Gamma Tracking) Code Developed Within the TMR (Training and Mobility through Research)

Program 'Gamma-ray Tracking Detectors' for the MARS Prototype detector (see e.g. Th. Kröll *et al.*, Eur. Phys. J. A **20**, 205 (2003)).

[25] N. Pietralla, Phys. Rev. C **59**, 2941 (1999).

[26] M. Krzysiek *et al.*, Acta Phys. Pol B **47**, 859 (2016).

[27] J. D. Sherman, D. L. Hendrie, and M. S. Zisman, Phys. Rev. C **15**, 903 (1977).

[28] R. M. Steffen and K. Alder, in *Angular Distributions and Correlations of Gamma Rays The Electromagnetic Interaction in Nuclear Spectroscopy*, edited by J. H. Hamilton (North Holland, Amsterdam, 1975).

[29] I. J. Thompson *et al.*, Comput. Phys. Rep. **7**, 167 (1988).

[30] D. Horen, R. L. Auble, J. R. Beene, F. E. Bertrand, M. L. Halbert, G. R. Satchler, M. Thoennessen, R. L. Varner, V. R. Brown, P. L. Anthony, and V. A. Madsen, Phys. Rev. C **44**, 128 (1991).

[31] T. P. Sjoreen, F. E. Bertrand, R. L. Auble, E. E. Gross, D. J. Horen, D. Shapira, and D. B. Wright, Phys. Rev. C **29**, 1370 (1984).

[32] W. Kim, B. L. Miller, J. R. Calarco, L. S. Cardman, J. P. Connelly, S. A. Fayans, B. Frois, D. Goutte, J. H. Heisenberg, F. W. Hersman, V. Meot, T. E. Milliman, P. Mueller, C. N. Papanicolas, A. P. Platonov, V. Yu. Ponomarev, and J. E. Wise, Phys. Rev. C **45**, 2290 (1992).

[33] E. Litvinova, P. Ring, and V. Tselyaev, Phys. Rev. C **78**, 014312 (2008).

[34] E. Litvinova, P. Ring, V. Tselyaev, and K. Langanke, Phys. Rev. C **79**, 054312 (2009).